coatings

MDPI

Article

Investigations into Power Plant Alloys' (Inconel 718) Oxidation Resistance by Compound Composite (Cr_2O_3 + YSZ) Coatings

Mohammed Yunus [1,*], Rami A. Alfattani [1], Turki Alamro [1] and Mohammed Asadullah [2]

[1] Department of Mechanical Engineering, Umm Al-Qura University, Makkah City 24372, Saudi Arabia
[2] Department of Mechanical Engineering, KNS Institute of Technology, Bengaluru 560064, India
* Correspondence: myhasan@uqu.edu.sa or yunus.mohammed@rediffmail.com

Abstract: As it increases the pressure and temperature of incoming steam and decreases CO_2 emissions, oxidation is crucial for materials used in power plants to increase their efficiency. Compound composite (Cr_2O_3 + YSZ) coatings applied to Inconel 718 (EN8) substrates using the Atmosphere Plasma Spray technique are anticipated to increase structural resistance when subjected to high pressure and temperature oxidation conditions of service. The nickel-based superalloys EN8 and EN8/Yttria (8% Y_2O_3) Stabilized Zirconia (YSZ)/Cr_2O_3 were subjected to high-temperature oxidation tests in the open air at 1050 °C for approximately 12, 24, 48, and 100 h. EN8 is not appropriate for prolonged use at 1050 °C as can be seen from scanned electron microscope and energy dispersive X-ray spectroscopy analyses on isothermally oxidized samples. The findings demonstrated that the EN8 alloy exhibited more significant weight variations over 48 h at high temperatures because its chromia oxide scale was continuously smaller. With phase dispersion in the microstructure, coated EN8 exhibits a higher performance under more prolonged exposure than the EN8 alloy. Additionally, the synthesis of outer chromium oxide, YSZ, and Cr_2O_3 on a substrate at 1050 °C for 100 h improved the outstanding oxidation resistance while maintaining the integrity of the chromium oxide layer.

Keywords: thermal barrier coating; yttria stabilized zirconia; Cr_2O_3; atmospheric plasma spraying; hot corrosion; oxidation resistance; Inconel 718

check for updates

Citation: Yunus, M.; Alfattani, R.A.; Alamro, T.; Asadullah, M. Investigations into Power Plant Alloys' (Inconel 718) Oxidation Resistance by Compound Composite (Cr_2O_3 + YSZ) Coatings. *Coatings* **2023**, *13*, 744. https://doi.org/10.3390/coatings13040744

Academic Editor: Heping Li

Received: 19 February 2023
Revised: 30 March 2023
Accepted: 2 April 2023
Published: 6 April 2023

Copyright: © 2023 by the authors. Licensee MDPI, Basel, Switzerland. This article is an open access article distributed under the terms and conditions of the Creative Commons Attribution (CC BY) license (https://creativecommons.org/licenses/by/4.0/).

1. Introduction

Enhancing corrosion resistance with superalloy materials used in high-temperature resistant zones is necessary to safeguard turbine components (compressor and combustion chambers) from erosion at operating temperatures. Superalloy materials deal with several issues that are surface-related. Superalloys based on nickel provide outstanding strength, toughness, and resistance to deterioration at higher temperatures in corrosive or oxidizing conditions and are suitable for use in nuclear power plants, aircraft, defense, turbines, and other industries. Tungsten, which is extensively used in nuclear fusion reactors, is prone to oxidation at high temperatures. When a reactor loses cooling, the tungsten armor is quickly oxidized and volatilized as air enters the vacuum chamber, resulting in disastrous nuclear leaks. The use of different alloys and coatings in the oxidation protection of tungsten, their microstructure, oxidation behavior, and failure causes are discussed. The path and tendency of oxidation protection of W-based materials are anticipated [1,2]. Iron and cobalt compositions are added to a superalloy to stabilize its structure; nickel, in particular, can enhance this property. The superalloy Inconel 718 (EN8), with appropriate modifications for application, covers a wide range of material compositions and mechanical strengths. At a high operating temperature, Ni and Cr protect the materials against surface damage such as corrosion, oxidation, and erosion. To increase strength and corrosion resistance, EN8 alloys include materials such as Al, Ti, Nb, Co, Cu, and W. Fe content in the alloys varies from 1% to 20% [3].

A critical concern with gas turbines (GT) is the development of materials for their components to minimize degradation, improve efficiency and life cycles, and reduce emissions [4]. The components of land-based GT and aircraft engines operate in challenging circumstances with high temperatures, leaving them susceptible to corrosion (which is caused by moist deposits of salts and acids such as chloride and sulfides). Corrosion is more common with heavy fuel oils than with natural gas because heavy fuel oils include impurities and additives that deposit aggressive combustion byproducts. Burning gasoline results in fast oxidation or corrosion because of environmental impurities in addition to hot air (sulfur, chlorine, and vanadium are examples of pollutants). The effects of continued exposure, particularly on substances used in GT, include severe thermal cycling [5]. The substances referred to as superalloys were developed for usage in high-temperature applications. Due to the scarcity of high-quality fuel and to the low cost of heavy oils, these oils are primarily employed as an energy source. When the surface of a metal reacts chemically with airborne oxygen, this is known as oxidation. The surface oxide layer may be detrimental or helpful as a barrier for protection against spallation or cracking. Erosion in GT is when solid or liquid particles contact rotating or stationary surfaces and remove material. Solid particles are created during the combustion of hydrocarbons and crushed coal [6].

Thermal barrier coating (TBC)s are designed to shield any substance from surface-based atmospheric processes such as corrosion, erosion, and others. Using Scanning electron microscope (SEM), Transmission electron microscope, Atomic force microscope, and Electron backscatter diffraction methods, a correlation between hot dip silicon-plating (HTSP) process factors and tungsten disilicide coating characteristics such as surface and interface morphologies, roughness, and texture has been established. Due to vigorous bombardment from high-energy Si ions, which prevents the formation of the lowest-energy crystal plane orientation, the coating comprises two layers, WSi_2 (outer) and W_5Si_3 (interface). The particle distribution on the coating surface is homogeneous, with minor surface roughness [7]. Utilizing an HTSP method, $MoSi_2$ and Si-$MoSi_2$ hybrid films with small $MoSi_2$ particles and higher surface silicon contents are applied to TZM (Mo-0.5Ti-0.1Zr-0.02C) metal. The diffusion layer is divided into three levels between 15 and 30 min of formation, with the first being $MoSi_2$ and Mo_5Si_3C (Si-$MoSi_2$, $MoSi_2$, and Mo_5Si_3). By decreasing stress mutation between the coating and the base, the gradient structure can further lessen the likelihood of crack spread. A silica layer coats a substantial portion of $MoSi_2$ grains when the deposition time is longer than 10 min, producing a very low coating surface [8]. Nickel, nickel-iron, nickel-cobalt, and other materials are used with NiCrAlY or NiCoCrAlY as the bond coat (BC). When the turbine's working temperature is around 700 °C, Thermally Grown Oxide (TGO) is the intermediate oxide scale below the topcoat and is exposed to increased temperature [9].

The bond coat helps shield the base substance from the corrosive medium and is made of an improved aluminide alloy such as MCrAlY (or any other in combination) [10]. The component's coating begins to peel off, revealing the surface of the underlying material, which promotes oxidation or melting. Multiple factors contribute to the failure, and TGO growth exceeds a threshold thickness, resulting in spall and TBC failure [11]. Fuel and sodium chloride are only two of the many factors that can lead to heat corrosion in superalloy materials when they are in use [12]. In the aviation and power generation industries, superalloys based on nickel are frequently used because of their increased strength and resistance to corrosion/oxidation at high temperatures [13]. Surface treatment is crucial for the GT parts to function better and last longer.

The exterior surfaces of GT parts that might be exposed to salt and high temperatures can be shielded by special coatings. Coatings protect against surface cracking, heat flux loading, cyclic fatigue, and compressor erosion. A larger aluminum content produces aluminum oxide, an additional layer of protection that significantly boosts resistance to oxidation at high temperatures [14]. Coatings help avoid surface erosion, corrosion, and tribo-corrosion at higher operating temperatures. The coating material (powder, grit, solid,

and liquid form) is heated up and propelled toward the substrate using numerous layers of coating with the help of a high-temperature and high-velocity gas steam.

Coatings incorporate minor components (such as Zr, Ta, Re, Hf, Pt, etc.) to boost their ability to resist corrosion. Aluminizing or coating ceramic materials produce TBCs with MCrAlY or YSZ to diffuse them with low heat conductivity [15]. A bond coat can be applied using atmospheric plasma spray (APS), while the topcoat is deposited using high-velocity oxyfuel. A great deal of research has been carried out on the evaluation of TBCs. Three factors—pressure, temperature, and environment—can be key determinants of a gas turbine engine's performance. This paper attempts to characterize the behavior of superalloy EN8 coated with composite materials.

Additionally, suggestions based on research will be made for coatings on GT parts that will increase those parts' resistance to oxidation and heat corrosion. EN8 has a basic character at lower temperatures owing to the emission of oxygen ions when the metal absorbs sulfur. Therefore, it can target ionic oxides, Cr_2O_3, and YSZ. YSZ is more resistant to acid fluxing and Cr_2O_3 is more resistant to basic fluxing. Many scholars have previously addressed superalloys' severe oxidation and corrosion behavior for specific applications. This study varies from previous studies regarding substance and simulation conditions. The coating layer was consistently maintained at 250 microns across all samples. High-temperature surface oxidation behavior studies on EN8 and composite APSed (Cr_2O_3 + 8% YSZ) EN8 were performed in this paper at 1050 °C. The samples were exposed to air directly for 24, 48, 96, and 100 h before being compared. The exposed samples were further investigated using metallurgical categorization techniques so the results could be illustrated more clearly and then discussed.

2. Methods and Materials

2.1. Experimental Setup

This section discusses the EN8 material selected for the investigation, its composition, and the coating procedure that involved thermal spraying with Cr_2O_3 and YSZ (with 8% yttria) powder. A detailed breakdown of the parameters and characteristics of the APS (thermal spray coating) were chosen. In addition, studies on corrosive environments and high thermal oxidation were included. The procedures, temperature, and salinity environment used for the hot corrosion investigations are also covered in this section. A few assessment methods used to evaluate oxidation and high-temperature oxidation include weight loss measurement, research into corrosion kinetics, and surface morphology investigations using SEM, EDS, and mass changes.

2.2. Materials Selection

This research aimed to examine the behavior of a potentially helpful material proposed in for high-temperature applications that simulate a high-temperature oxidation environment. Tables 1 and 2 show the chemical composition of base substance EN8, and coats (such as the bond, inner, and exterior ceramic coats) are listed.

Table 1. Lists the chemical composition of the investigational EN8 material.

EN8	Ni	Fe	Cr	Nb	Mo	Ti	Al	Si	C	Co	Cu & W
In wt%	54	17.26	18	5.31	3.03	0.96	0.56	0.09	0.005	0.16	0.350 & 0.278

Table 2. Lists the chemical composition of the exterior, inner, and bond coats.

Materials	Zr (wt%)	Cr (wt%)	Ni (wt%)	O (wt%)	Y (wt%)	Al (wt%)
YSZ (Inner)	68.1	-	-	28.7	3.2	-
Cr_2O_3 (Exterior)	-	74	-	26	-	-
NiCrAlY (bond)	-	15–25	59.5–74.8	-	0.2–0.5	10–15

2.3. Sample Preparation for Coatings

The cast materials EN8 were cut precisely with an abrasive water jet to prevent surface flaws such as recast layer, heat affected zone (HAZ), and other thermal fatigues brought on by machining. The samples were made to meet the necessary $30 \times 10 \times 3$ mm^3 dimensions for thermal spray deposition. A collection of samples was mechanically polished (in the range of 600 to 1200 grit) using emery paper of various grit sizes to produce a mirror shine More alumina polishing was carried out in order to avoid micro scars. Following acetone cleaning, heated air drying was used. The base material's behavior without an APS coating was examined in this way, creating metallurgical samples at a high temperature that simulates a mixed salt environment and air.

2.4. Thermal Spray Coatings (TSC)

A few basic procedures must be followed to apply thermal spray coatings to base metals. Before drying in hot air for plasma coating, the samples' surfaces were cleaned with acetone to remove foreign objects. Next, the samples were made using an advanced machining technique that naturally produces a damage-free surface of a quality which achieves the best coating adhesion. For the best coatings, the sample surfaces had to be between 7 and 10 µm rough [16]. Prior to coating, the samples were warmed to 250 °C. The EN8 materials received a coating of YSZ and chromium oxide powder that was applied using the atmospheric plasma spray (APS) technique after being thermally sprayed to a 60 (YSZ):40 (Cr_2O_3) weight-per-percent coating of each substance. The article sizes of the coating powder's amorphous, irregularly shaped particles range from 30 to 35 µm. Each of the six faces of the substrate has a coating with a thickness of 250 µm.

The specimens were cleaned with acetone after polishing with silicon carbide emery paper with a 1500 grit setting. Each sample's initial weight and surface area were collected before the oxidation test. Using a vernier caliper, the surface areas of the specimens were measured, and the initial weight was measured on a precision balance with three-decimal accuracy. Through the use of an APS technique and a METCO USA 3MB gun on the prepared EN8 samples, the bond (NiCrAlY), inner (YSZ), and exterior (Cr_2O_3) ceramic coatings were sequentially deposited as per the spraying specifications (Table 3) with an interval of less than one hour between each coating. With Cr_2O_3 and YSZ powder particles of approximately 35 µm in size, the coating thickness for all samples was kept almost uniform (250 µm). Throughout all coating processes, these spray parameters remained constant. Prior to spraying, the substrate alloys were grit-blasted with Al_2O_3 (to a depth of about 150 µm) for improved coating adhesion.

Table 3. Spraying parameters of APS process.

S. No.	Spray Settings	Spraying Condition	Units
1	Plasma-Arc-current	500	A
2	Arc-Voltage	65–75	V
3	Plasma Gas (Argon) Flow rate	78–90	L/min
4	Secondary gas (Hydrogen) Flow rate	1.8–2.4	L/min
5	Plasma Gas (Argon) Pressure	0.70–0.80	MPa
6	Secondary gas (Hydrogen) Pressure	0.35	MPa
7	Power feed rate	39.6–50	g/min
8	Torch to base (standoff) distance	100–125	mm

2.5. High-Temperature Oxidation

Oxidation tests were conducted in an intensified heating tubular furnace at 1050 °C for 24, 48, and 100 h, with temperature stability and timing managed by an embedded PID control system. A 5 °C increase in the furnace temperature occurred per minute. The EN8

material was subjected to oxidation tests for 100 h (in 20 cycles for 5 h as soaking time) at 900 °C and 1050 °C with a five-hour interval between each cycle. At 1050 °C, oxidation studies on the coated samples were also conducted. The medium used for oxidation studies is atmospheric air. The metallurgical characterization techniques and mass change per unit area are used to assess the material's behavior.

2.6. Testing and Evaluation

Following the experiment, the samples were examined and assessed regarding mass change per unit area ($\Delta m/mm^2$). Energy dispersive X-ray spectroscopy (EDS), optical images, and SEM images were used to analyze the surface morphology of the samples. Both the samples (with and without coating) underwent high-temperature oxidation, and each specimen's changing mass per unit area (m) was assessed. The microstructure and grain boundaries of the samples were examined using an optical microscope and an SEM. With the aid of an energy-dispersive spectrometer attached to a scanning electron microscope (Make: Zeiss, Jena, Germany), the surface morphology, including oxides, micropores, cracks, etc., was examined. The element weight proportions in the exposed sample cross-sections and on the oxide surface were categorized by EDS. EDS analysis was performed using Rigaku (Make: Brukers GmbH, Mannheim, Germany) radiation before and after oxidation. Images of the materials as received, deposited, and after oxidation were examined using a scanning electron microscope (Zeiss, Jena, Germany).

3. Results and Discussion

The YSZ/Cr_2O_3 coating applied to the EN8 substrate is shown in cross-sectional SEM images (Figure 1). The YSZ and Cr_2O_3 layers, along with the bond coat, have a thickness of 250 µm. No spallation occurred between the YSZ, Cr_2O_3, and bond coat layers. The top coating was made of chromium, and oxygen entities can react with air producing more CrO_2 and converting Cr_2O_3, maintaining the exterior coat and thus maintaining good contact with YSZ. The homogeneous structure and sporadic columnar gaps of both coated films give the coatings the impression of being porous.

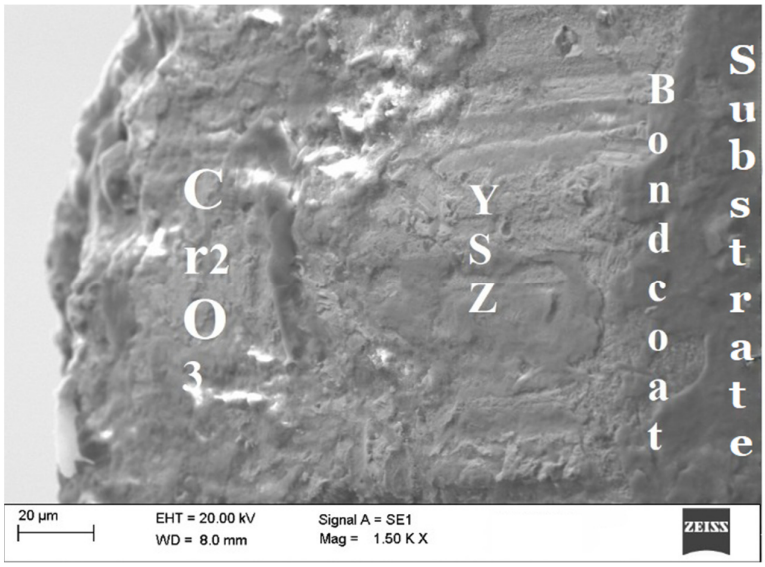


Figure 1. Shows a cross-sectional SEM of YSZ/Cr_2O_3 after deposition.

At 1000 °C, isothermal oxidizing experiments lasting 24, 48, and 100 h assessed each oxidation behavior of uncoated and coated (YSZ/Cr_2O_3) EN8 in addition to the development of the oxide scale. Figure 2 shows SEM images of EN8 after 100 h high oxidation.

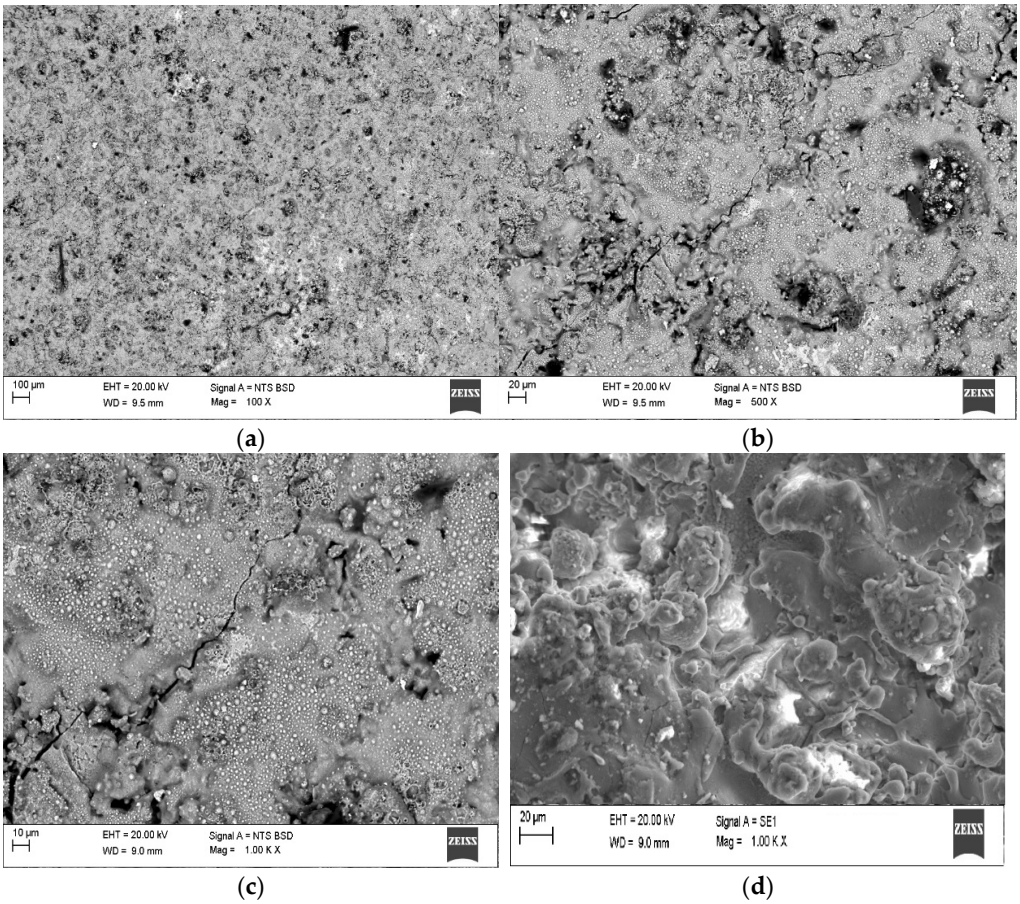


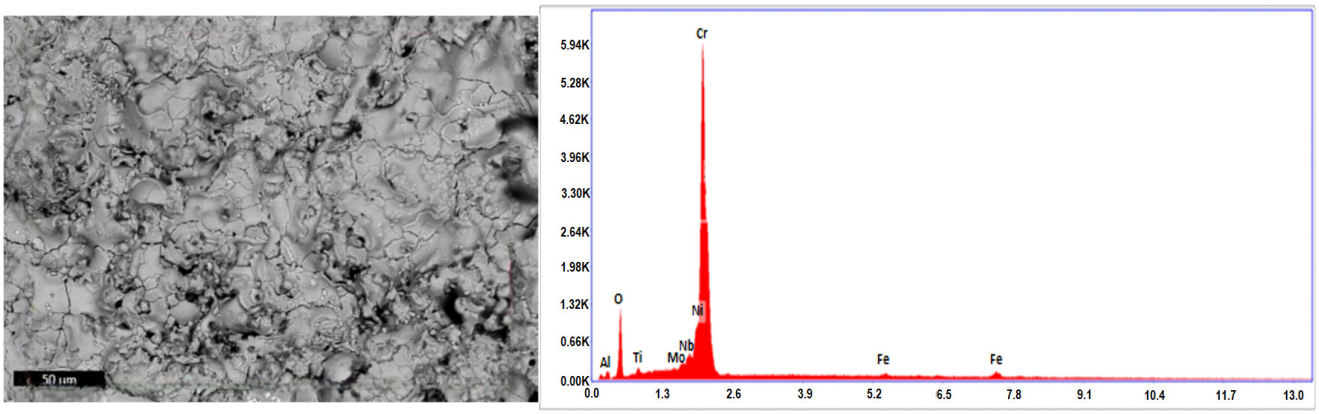
Figure 2. Morphology of coated EN8 after (**a**) 24 h, (**b**) 48 h, (**c**) 100 h hot oxidation, and (**d**) uncoated EN8 after 100 h hot oxidation (1050 °C).

The oxide film on coated EN8 tends to become thicker over time, as shown in Figure 2. Early in the oxidation process, deeper penetration is observed when the transient internal oxidation is considerably low. Each element originally produced its associated oxides through oxidation. As a result, the highest oxide layer thickness increases at this stage [9,10]. Following this phase, Cr_2O_3 predominately forms alongside other oxides.

Additionally, a zone of internal oxidation was seen beneath the surface. This suggests a linear oxidation kinetic for the conditions of the oxidation test in EN8. Due to the absence of aluminum and the presence of zirconia, 8% of YSZ structures are visible on the grain boundaries. Oxide layer formations are seen to separate in the later stages of oxidation (Figure 3). This is attributed to both the thermal growth disparity between the oxide forming and the base metal as well as the formation of a volatile CrO_3 phase at 1050 °C as a result of the Cr_2O_3's reaction with oxygen, which lessens the durability of the oxide film [17,18]. Except for 20 h, where the oxide layer thickness would be minimal, no accurate measurement of the oxide layer could be made due to the oxide layer cracking and separating with the increasing oxidation period. Over time, the internal oxidation depth also grows. When EN8 is subjected to 168 h of cyclic oxidation at 950 °C, the resulting average layer thickness will reach a maximum of 24 µm [19].

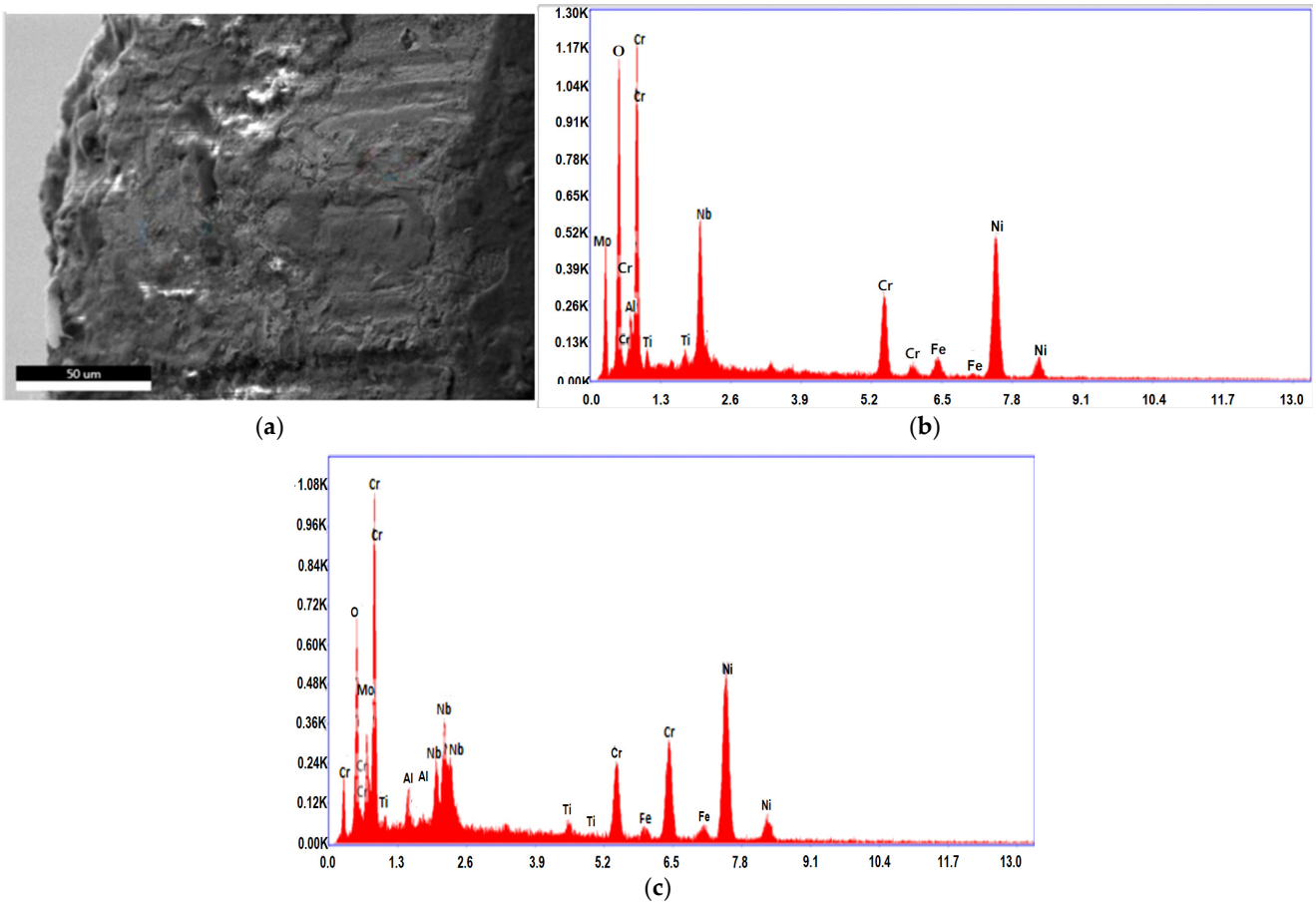
According to the findings, high-temperature oxidation had a significant impact on EN8. The elemental analysis images obtained after a 100 h oxidation period (Figure 4) show that Cr_2O_3 is the predominant phase in the topcoat. However, due to the extremely low percent and Al having a significantly greater affinity for oxygen than any other element, this, together with Al's melting point, allows it to keep its oxide state there even although Al_2O_3 only forms at the grain boundaries. As seen in the EDS analysis images, the elements that underwent oxidation after Cr are Mo, Nb, Zr, and Ti. Low Cr, high Ni, and Fe, and a

sliver of Mo are present in the lower regions of the oxide layer. Al, Ti, and Nb are almost all depleted because of oxidation in the area where the image was taken. The resulting oxide phases were identified using EDS analysis (Figure 5). In accordance with the lengthening of the oxidation process, other oxide formations joined the Ni, Fe, and Cr rich materials that were initially present on the EN8 in the results of the EDS analysis. Small quantities of oxides of different elements of EN8, along with the main Cr_2O_3 phase, were also formed throughout the 24-h oxidizing duration [20].



(**a**) (**b**)

Figure 3. Coated EN8 (**a**) SEM morphology and (**b**) EDS spectrum for isothermal oxidation after 12 h at 900 °C.



(**a**) (**b**)

(**c**)

Figure 4. Coated EN8 (**a**) SEM morphology and (**b**) EDS spectrum for isothermal oxidation after 100 h at 1050 °C and (**c**) EDS spectrum at 900 °C.

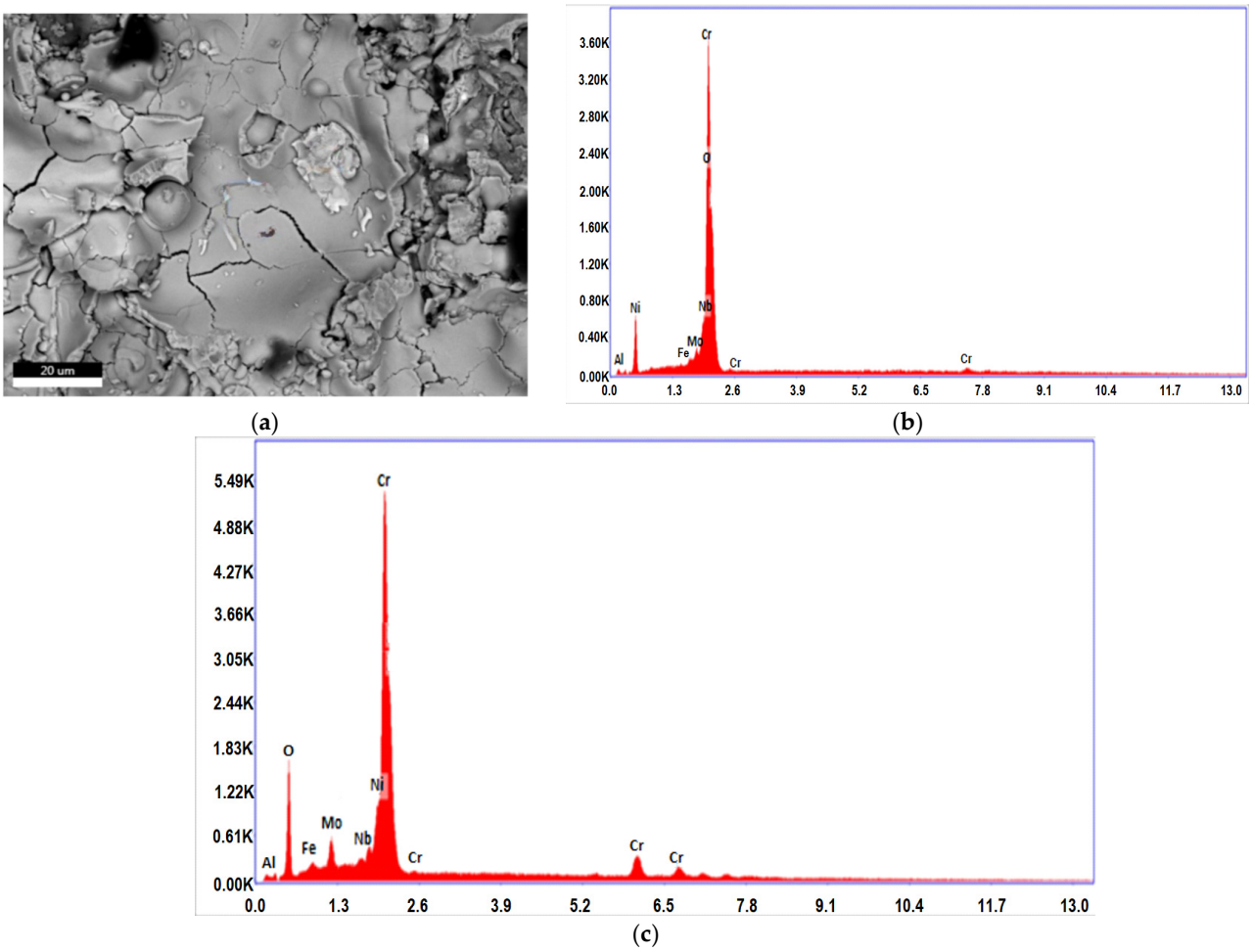


Figure 5. Coated EN8 (**a**) SEM morphology (**b**) EDS spectrum for isothermal oxidation after 48 h at 1050 °C and (**c**) EDS spectrum at 900 °C.

After varying oxidation times at 900 °C, it was discovered that Cr_2O_3 was the predominant phase; however, $CrNbO_4$ was present at first due to Nb diffusion from the grain boundaries (see Table 4). In contrast, inter-granular oxidation in Al and Ti, and Ni_3Nb intermetallic phase formations within the structure, have also been reported [3]. When coated, EN8 samples were exposed to oxidizing air for prolonged periods. It was also noted that Cr_2O_3 was the predominant phase, even after a 24 h oxidation period that only produced minor amounts of the phases Ni_3Al, NiO, $NiCr_2O_4$, TiO_2, and $TiNb_2O_7$ (Figure 6). Upon 100 h of oxidation, Cr_2O_3 continued to be the dominating phase along with the above phases. These formations were confirmed by comparing the results to the EDS data and the image depicted in Figure 4 [21].

Table 4. EDS Composition of coated EN8 for different oxidation times and at different temperatures.

Elements	Coated EN8 for 12 h at 900 °C (wt.%)	Coated EN8 for 24 h (wt.%)		Coated EN8 at 48 h (wt.%)		Coated EN8 at 100 h (wt.%)	
		At 900 °C	At 1050 °C	At 900 °C	At 1050 °C	At 900 °C	At 1050 °C
O	26.75	28.91	29.27	26.94	26.51	18.62	14.51
Ni	8.03	7.35	5.1	7.4	4.6	5.27	7.17
Nb	4.52	3.87	3.2	3.26	2.1	2.18	2.12
Mo	3.71	3.84	3.0	2.1	2.2	1.75	2.1
Ti	0.74	0.75	1.2	1.1	1.4	1.2	0.8
Cr	51.74	53.29	55.93	56.4	60.1	68.75	71.07
Fe	2.3	0.71	1.1	1.3	1.2	1.03	1.05
Al	2.2	1.3	1.2	1.5	1.89	1.2	1.1

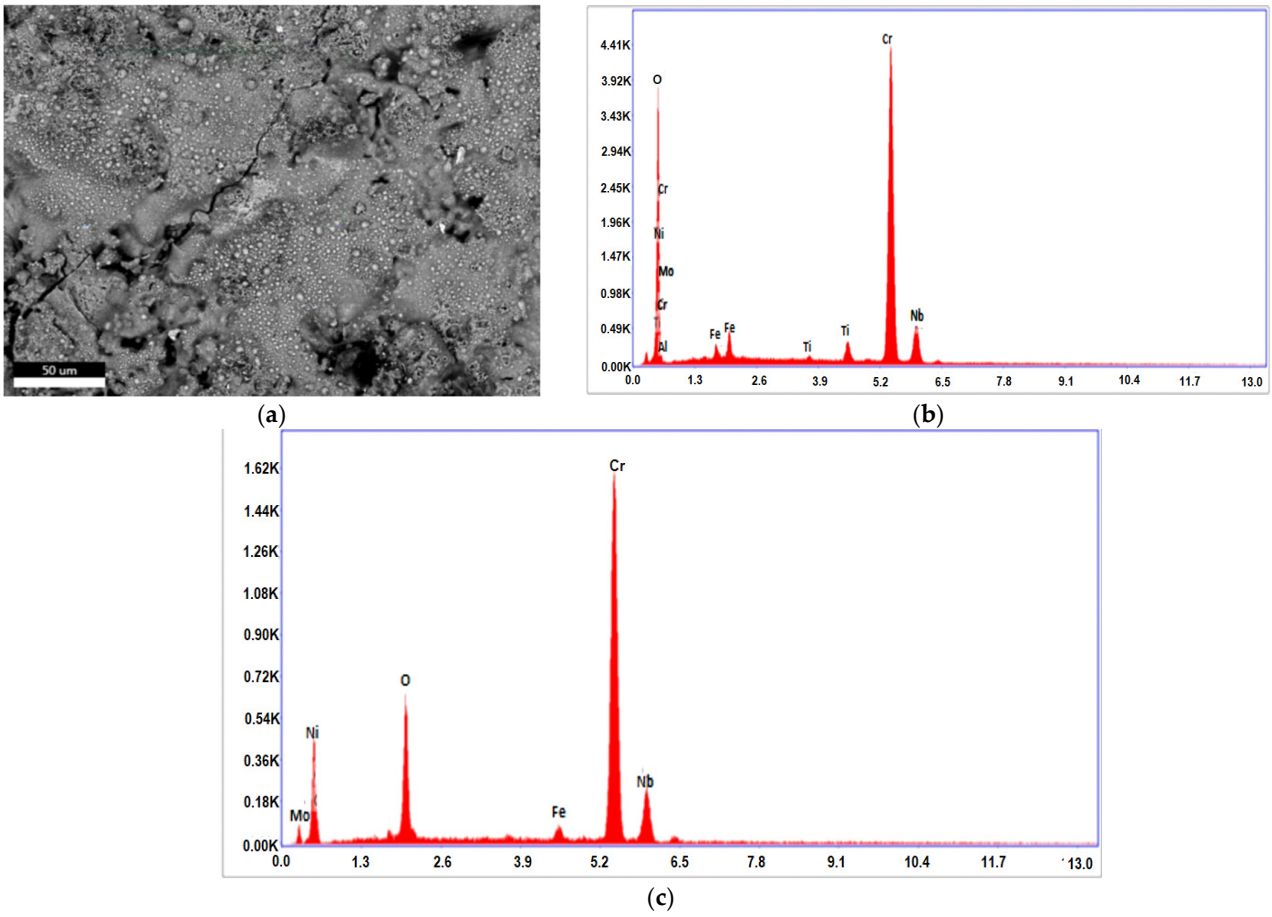


Figure 6. Coated EN8 (**a**) SEM morphology and (**b**) EDS spectrum for isothermal oxidation after 24 h at 1050 °C and (**c**) EDS spectrum at 900 °C.

At the oxidation temperatures used in this study, EN8 demonstrates constant propagation-regulated parabolic gradient characteristics. Above 1200 °C, it is claimed to distort simply through its self-weight, and the dynamical oxidizing stage can last up to 24 h at minimal temperatures (Figure 3) [22]. However, in this study, as can be inferred from the results of the EDS analysis and the reports of spinel formation, segments were observed both during the early stages and extended periods of oxidation at the inner regions of the structure but were found to last less than 20 h. In contrast, after a day (24 h) and at 100 h of oxidation, EDS findings demonstrated the NiO phase as a result of high temperature.

An 100 h oxidation of EN8 at 850 °C revealed that Cr_2O_3 was the predominant phase with Ni (Cr, Fe)$_2O_4$ spinel phases present at trace levels. Stresses brought on by expanding oxides led to the oxide layer spalling, something which is similar to this study [23]. During this study no coated EN8 samples showed any evidence of spalling oxidized films. The substrate/coating and YSZ//Cr_2O_3 interfaces did not exhibit spallation (Figure 6). A significantly smoother columnar growth was produced by low interface roughness, as oxygen ions pass through the coating at high-temperature permeability towards ions in the coating materials; therefore, EN8 is oxidized at the coating interface [24]. After a 24 h oxidation period, the results of the EDS showed that, at contact, Cr_2O_3 predominates. Mo, Nb, and Ti also experienced minor quantities of oxidation (Figure 5). Based on the EDS analysis, it was determined that $TiNb_2O_7$ and Cr (Mo, Nb) O_4 were the phases most likely to emerge. After 24 h, the resulting phases resemble those seen after 20 h of oxidation, with the thicker oxide layer and the predominant phase still being Cr_2O_3. Columnar spalling and cracking near the top interface coat were seen after a 100 h oxidation period. The EDS examination indicates that Cr_2O_3 is the predominant phase, with tiny quantities of Fe, Mo, Nb, Ti, and Al oxides. During the 100 h of oxidation of EN8 at 1050 °C, the oxide stages of various elements of the EN8 was produced. Coated samples offered better resistance than uncoated EN8 due to the applied coating materials' low thermal conductivity and the reduced partial pressure of oxygen.

EDS analysis confirmed the distribution of the resulting oxide structures. Despite chemical compatibility, the produced coatings and the resulting oxides did not react. The volatile CrO_3 phase changed to Cr_2O_3 when it reacted with oxygen, which was not formed because of the thermal insulation that the YSZ/Cr_2O_3 coating provided, and no new phase developed after the coating had been exposed to oxygen for 100 h. Since Cr_2O_3 is phase-stable up to 1500 °C, the structure did not undergo any phase transition. The combination of YSZ and/or Cr_2O_3 produces the best results for high-temperature failures in TBC-related studies [25,26]. While Cr_2O_3 has a higher sintering resistance, lower oxygen permeability, and lower thermal expansion, the thermal coefficient of expansion (CTE) and fracture toughness (FT) of YSZ are higher [27]. When the coating oxidizes, a considerable amount of stress is generated at the interface between it and the base metal. To correct the mismatch between oxidative stress and thermal growth, YSZ is used. Single film Cr_2O_3 is inappropriate because of its reduced CTE and lower values for FT. Additionally, the formed oxides and Cr_2O_3 can react, and at the interface, brittle phases will be formed [17,28]. Contrasted with/Cr_2O_3 single layer, YSZ is more appropriate.

In this study, the oxide film that was created following the oxidative testing of EN8 showed signs of cracking and delamination, but this was avoided by using the YSZ/Cr_2O_3 coat. When the process of forming oxides and their growth characteristics is considered, it is clear that bond coating is a better option. In experiments comparing the oxide film thicknesses and the growing tendency, TBCs containing bond covering outperformed this study [17,29]. Nevertheless, it is thought that alterations to the substrate might improve the performance of the coating scheme even in the absence of a BC.

At 900 and 1050 °C, the EN8's high-temperature oxidizing behavior was evaluated by exposing it to atmospheric air (refer to Figure 7). When in contact with air, the specimen exhibits a good oxidation barrier. During the corrosion studies at 900 and 1050 °C, the specimens of uncoated and coated EN8 underwent small variations in mass of less than 1 mg/cm^2 and 2.7 mg/cm^2, respectively. According to researchers, all nickel-based superalloys exhibit excellent oxidation and hot corrosion resistance at about 900 °C and therefore show gradual mass changes without fluctuation [9,10,30]. On the other hand, coated EN8 also exhibits good oxidation and hot corrosion resistance up to 1050 °C. As opposed to this, at 1050 °C, the identical samples behaved similarly, with initial broad variances in mass changes accumulating over the following cycles.

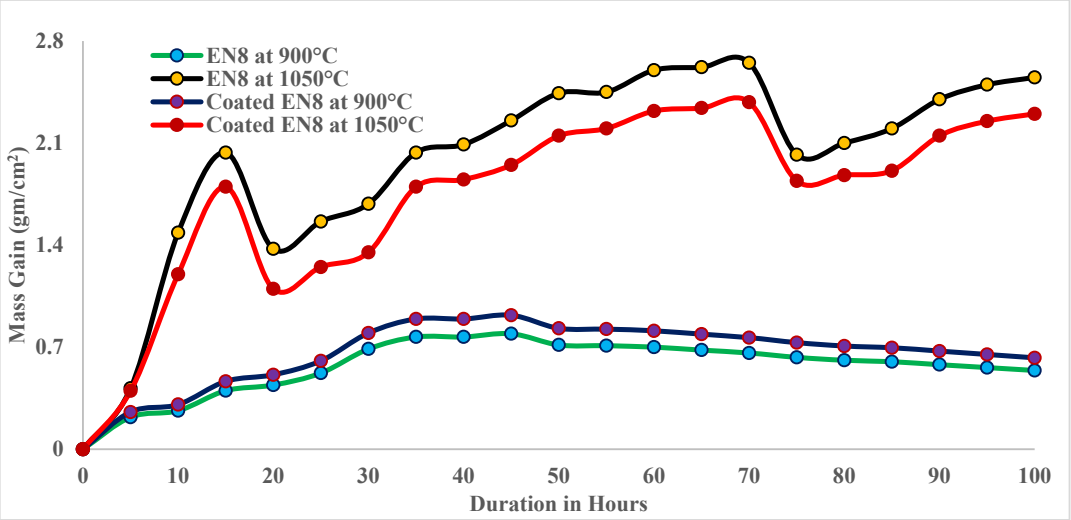


Figure 7. EN8's mass gain vs. oxidation duration before and after deposition.

The mass change average per square centimeter is 1.65 mg. At first, there was a noticeable change, and it continued for 15 h. EN8 observed a higher rate of mass gain for the coated alloys during the initial oxidation cycle due to the active element oxides rapidly forming and oxidizing at the coating splat boundaries and the oxidizing species penetrating along the splat boundaries/open pores. However, the coating's oxide scale thickened, and the diffusion of oxidizing species into its interior slowed down as soon as oxides formed at the pore and splat boundaries. Comparatively, this would result in lower mass gain during progressive cycles, highlighting the parabolic nature of both coated alloys.

4. Conclusions

In experimental research, physical and metallurgical changes are examined to gauge the behavior of EN8 and EN8 coated with YSZ-Cr_2O_3 powder using the plasma spraying method at elevated temperatures of 900° and 1050 °C for 24, 48, and 100 h in atmospheric air to simulate a GT environment. The material characterization studies using SEM and EDS produced the following results based on the experiment.

High-temperature oxidation does not alter EN8 main phases considerably at 900 °C. However, due to the alloy's affinity during oxidation, the sample displayed catastrophic behavior above 1050 °C. After oxidation tests, it was discovered that Cr_2O_3 was the primary phase in EN8 and that the internal oxidation and oxide layer thickness increased with time. After 100 h of oxidation testing, separating was seen as a consequence of pressure caused by oxide production and thermal gradient lag. As a result, the oxide structure's growth behavior at the interface could be seen clearly. The findings indicate that EN8 needs to be modified in order to exhibit excellent oxidation resistance. It was determined that EN8 is unsuitable because it produces rapidly evolving mixed oxides over long oxidation periods at 1050 °C. Applying the ceramic protective film improved EN8's resistance to oxidation and stopped oxide delamination. There was no indication during the oxidizing tests that the coating structure had undergone a phase change or that the coated layer and the EN8 were chemically mismatched. Due to the reduced stresses of the oxides and the associated thermal growth, the coating layer showed no signs of columnar separation after 100 h of oxidation. Due to its high melting point, it inhibits chromium diffusion during oxidation and encourages the formation of a protective phase beneath the coating, such as spinels rich in nickel and chromium.

The surface of EN8 can be changed in upcoming studies by adding more YSZ (zirconium) or Cr_2O_3 (chromium oxide). In addition, it is hoped that future research will add Cr_2O_3 to EN8's surface to create alloys that will enhance EN8's high-temperature

performance. With Al_2O_3 and Cr_2O_3 coatings, the oxidation resistance of these rare earth element oxide alloys can be further improved.

Author Contributions: Conceptualization, M.Y., T.A. and M.A.; Methodology, M.Y., R.A.A. and M.A.; Software, T.A. and M.A.; Validation, R.A.A.; Formal analysis, M.Y. and M.A.; Investigation, M.Y.; Resources, R.A.A.; Data curation, T.A.; Writing—original draft, M.Y.; Writing—review & editing, R.A.A., T.A. and M.A.; Visualization, T.A.; Supervision, M.Y. and M.A.; Project administration, M.Y. and R.A.A.; Funding acquisition, R.A.A. All authors have read and agreed to the published version of the manuscript.

Funding: The authors extend their appreciation to the Deputyship for Research & Innovation, Ministry of Education in Saudi Arabia for funding this research work through project number: IFP22UQU4310022DSR096.

Institutional Review Board Statement: Not applicable.

Informed Consent Statement: Not applicable.

Data Availability Statement: The data analyzed in this manuscript is the part of our research work and is available for public use.

Conflicts of Interest: The authors declare no conflict of interest.

References

1. Fu, T.; Cui, K.; Zhang, Y.; Wang, J.; Shen, F.; Yu, L.; Qie, J.; Zhang, X. Oxidation Protection of Tungsten Alloys for Nuclear Fusion Applications: A Comprehensive Review. *J. Alloys Compd.* **2021**, *884*, 161057. [CrossRef]
2. Pollock, T.M.; Tin, S. Nickel-Based Superalloys for Advanced Turbine Engines: Chemistry, Microstructure and Properties. *J. Propuls. Power* **2006**, *22*, 361–374. [CrossRef]
3. Thomas, A.; El-Wahabi, M.; Cabrera, J.M.; Prado, J.M. High Temperature Deformation of Inconel 718. *J. Mater. Process. Technol.* **2006**, *177*, 469–472. [CrossRef]
4. Wright, I.; Gibbons, T. Recent Developments in Gas Turbine Materials and Technology and Their Implications for Syngas Firing. *Int. J. Hydrog. Energy* **2007**, *32*, 3610–3621. [CrossRef]
5. Al-hatab, K.A.; Al-bukhaiti, M.A.; Krupp, U.; Kantehm, M. Cyclic Oxidation Behavior of in 718 Superalloy in Air at High Temperatures. *Oxid. Met.* **2010**, *75*, 209–228. [CrossRef]
6. Mishra, T.; Datta, A.; Mukhopadhyay, A. Comparison of the Structures of Methane–Air and Propane–Air Partially Premixed Flames. *Fuel* **2006**, *85*, 1254–1263. [CrossRef]
7. Zhang, Y.; Fu, T.; Cui, K.; Shen, F.; Wang, J.; Yu, L.; Mao, H. Evolution of Surface Morphology, Roughness and Texture of Tungsten Disilicide Coatings on Tungsten Substrate. *Vacuum* **2021**, *191*, 110297. [CrossRef]
8. Zhang, Y.; Cui, K.; Fu, T.; Wang, J.; Shen, F.; Zhang, X.; Yu, L. Formation of $MoSi_2$ and $Si/MoSi_2$ Coatings on TZM (Mo–0.5Ti–0.1Zr–0.02C) Alloy by Hot Dip Silicon-Plating Method. *Ceram. Int.* **2021**, *47*, 23053–23065. [CrossRef]
9. Basha, A.K.M.; Srinivasan, S.; Srinivasan, N. Studies on Thermally Grown Oxide as an Interface between Plasma-Sprayed Coatings and a Nickel-Based Superalloy Substrate. *Int. J. Miner. Metall. Mater.* **2017**, *24*, 681–690. [CrossRef]
10. Chellaganesh, D.; Khan, M.A.; Winowlin Jappes, J.T. High Temperature Oxidation Behavior of Thermally Sprayed Alumina—Titania Coatings on Nickel Based Superalloys. *Mater. Res. Express* **2019**, *6*, 086521. [CrossRef]
11. Asadullah, M.; Bhagyashekar, M.S.; Yunus, M. RSM Multi-Properties Optimization of Various Input Factors of Thermal Barrier Composites. *Multiscale Multidiscip. Model. Exp. Des.* **2021**, *5*, 67–80. [CrossRef]
12. Lai, G.Y. *High-Temperature Corrosion and Materials Applications*; ASM International: Novelty, OH, USA, 2007.
13. Wang, P.; Deng, S.; He, Y.; Liu, C.; Zhang, J. Oxidation and Hot Corrosion Behavior of Al_2O_3/YSZ Coatings Prepared by Cathode Plasma Electrolytic Deposition. *Corros. Sci.* **2016**, *109*, 13–21. [CrossRef]
14. Yuan, L.; Hu, R.; Zhang, T.; Han, Y.; Xue, X.; Li, J. Precipitation Behavior of σ-FeCr Phases in Hastelloy C-2000 Superalloy under Plastic Deformation and Aging Treatment. *J. Mater. Eng. Perform.* **2014**, *24*, 565–571. [CrossRef]
15. Doleker, K.M.; Odabas, O.; Ozgurluk, Y.; Askerov, H.; Karaoglanli, A.C. Effect of High Temperature Oxidation on Inconel 718 and Inconel 718/YSZ/$Gd_2Zr_2O_7$. *Mater. Res. Express* **2019**, *6*, 086456. [CrossRef]
16. Sun, L.; Berndt, C.C.; Gross, K.A.; Kucuk, A. Material Fundamentals and Clinical Performance of Plasma-Sprayed Hydroxyapatite Coatings: A Review. *J. Biomed. Mater. Res.* **2001**, *58*, 570–592. [CrossRef]
17. Doleker, K.M.; Ozgurluk, Y.; Ahlatci, H.; Karaoglanli, A.C. Evaluation of Oxidation and Thermal Cyclic Behavior of YSZ, $Gd_2Zr_2O_7$ and YSZ/$Gd_2Zr_2O_7$ TBCs. *Surf. Coat. Technol.* **2019**, *371*, 262–275. [CrossRef]
18. Zhang, T.; Huang, C.; Lan, H.; Du, L.; Zhang, W. Oxidation and Hot Corrosion Behavior of Plasma-Sprayed MCrAlY–Cr_2O_3 Coatings. *J. Therm. Spray Technol.* **2016**, *25*, 1208–1216. [CrossRef]
19. Jian, L.; Yuh, C.Y.; Farooque, M. Oxidation Behavior of Superalloys in Oxidizing and Reducing Environments. *Corros. Sci.* **2000**, *42*, 1573–1585. [CrossRef]

20. Greene, G.A.; Finfrock, C.C. Oxidation of Inconel 718 in Air at High Temperatures. *Oxid. Met.* **2001**, *55*, 505–521. [CrossRef]
21. Delaunay, F.; Berthier, C.; Lenglet, M.; Lameille, J.-M. SEM-EDS and XPS Studies of the High Temperature Oxidation Behaviour of Inconel 718. *Microchim. Acta* **2000**, *132*, 337–343. [CrossRef]
22. Jia, Q.; Gu, D. Selective Laser Melting Additive Manufactured Inconel 718 Superalloy Parts: High-Temperature Oxidation Property and Its Mechanisms. *Opt. Laser Technol.* **2014**, *62*, 161–171. [CrossRef]
23. Fox, A.C.; Clyne, T.W. Oxygen Transport by Gas Permeation through the Zirconia Layer in Plasma Sprayed Thermal Barrier Coatings. *Surf. Coat. Technol.* **2004**, *184*, 311–321. [CrossRef]
24. Mahade, S.; Curry, N.; Björklund, S.; Markocsan, N.; Nylén, P. Thermal Conductivity and Thermal Cyclic Fatigue of Multilayered $Gd_2Zr_2O_7$/YSZ Thermal Barrier Coatings Processed by Suspension Plasma Spray. *Surf. Coat. Technol.* **2015**, *283*, 329–336. [CrossRef]
25. Leckie, R.M.; Krämer, S.; Rühle, M.; Levi, C.G. Thermochemical Compatibility between Alumina and ZrO_2–$GdO_3/2$ Thermal Barrier Coatings. *Acta Mater.* **2005**, *53*, 3281–3292. [CrossRef]
26. Adam Khan, M.; Sundarrajan, S.; Natarajan, S. Influence of Plasma Coatings on Inconel 617 for Gas Turbine Applications. *Surf. Eng.* **2014**, *30*, 656–661. [CrossRef]
27. Asadullah, M.; Yunus, M. Optimization of Coating Thickness for various Properties of Composite type Thermal Barrier Coated with INCONEL 718 Alloy. *High Temp. Mater. Process. Int. Q. High-Technol. Plasma Process.* **2019**, *23*, 377–389. [CrossRef]
28. Softah, G.J. Characterization and Performance Study of DCMD in Different Configurations after Membrane Thermal Treatment. *J. Umm Al-Qura Univ. Eng. Archit.* **2020**, *11*, 33–38.
29. Mohammed, W.A.; Ahmed, H.B. Influence of Infill density and Orientation on the Mechanical Response of PLA+ Specimens Produced using FDM 3D Printing. *Int. J. Adv. Sci. Technol.* **2020**, *29*, 3362–3371.
30. Padhan, S.; Das, S.R.; Das, A.; Alsoufi, M.S.; Ibrahim, A.M.M.; Elsheikh, A. Machinability Investigation of Nitronic 60 Steel Turning Using SiAlON Ceramic Tools under Different Cooling/Lubrication Conditions. *Materials* **2022**, *15*, 2368. [CrossRef]

Disclaimer/Publisher's Note: The statements, opinions and data contained in all publications are solely those of the individual author(s) and contributor(s) and not of MDPI and/or the editor(s). MDPI and/or the editor(s) disclaim responsibility for any injury to people or property resulting from any ideas, methods, instructions or products referred to in the content.